Emergence of the South Atlantic Convergence Zone–ENSO connection under global warming

Jae-Heung Park (jhp11010@gmail.com)
Pohang University of Science and Technology https://orcid.org/0000-0002-8556-2314
Jong-Seong Kug
Division of Environmental Science and Engineering, Pohang University of Science and Technology
Young-Min Yang
Nanjing University of information science and technology
Hyo-Jin Park
Yonsei University
Geon-Il Kim
Pohang University of Science and Technology
Ji-Hoon Oh
Pohang University of Science and Technology
Chao Liu
Yonsei University
Soon-Il An
Yonsei University https://orcid.org/0000-0002-0003-429X

Article

Keywords:

Posted Date: October 6th, 2023

DOI: https://doi.org/10.21203/rs.3.rs-3376707/v1

Abstract

South America has been warming faster than the surrounding oceans in recent decades, leading to changes in its precipitation patterns, particularly the South Atlantic Convergence Zone (SACZ) in the subtropical region. Through an analysis of observational reanalysis datasets, this study reveals an emerging link between the SACZ in the boreal spring and El Niño–Southern Oscillation (ENSO) in the following winter. In recent decades, the variability of SACZ during boreal spring accompanies an anomalous precipitation dipole between tropical and subtropical South America, resulting in the development of a local meridional circulation. This convective activity over tropical South America, in turn, affects the Walker circulation over the Pacific, thereby influencing the evolution of ENSO events. Further analysis based on historical and future scenarios suggests that the lagged SACZ–ENSO connection is projected to be strengthened in the future, implying a high likelihood that the emergence of the observed connection in recent decades is attributable to anthropogenic forcing.

Main text

South America stands out as a climatologically distinctive continent characterized by the presence of two prominent convergence zones: the Atlantic intertropical convergence zone (ITCZ[1]) in tropics and South Atlantic convergence zone (SACZ[2,3]) in subtropics (Supplementary Fig. 1). The copious rainfall generated by these convergence zones accumulates in two key regions: the Amazon basin in tropical South America and the La Plata basin in subtropical South America. The unique climatological attributes of South America contribute to its profound ecological and socio-economic importance[4,5].

The active precipitation system[6,7] in the South America is tightly linked to the Pacific[8–10], Atlantic[7,11,12], and Africa[13] through atmospheric teleconnections operating at different timescales. For example, the precipitation in South America are significantly affected by both the tropical Pacific and Atlantic oceans, in association with interannual and decadal climate phenomena such as El Nino-Southern Oscillation (ENSO[14,15]), Atlantic-Nino[16,17], Interdecadal Pacific Oscillation (IPO[18]), and Atlantic Multidecadal Oscillation (AMO[19]). Conversely, the precipitation in South America also holds the potential to impact the climate system of the tropical Pacific and Atlantic Oceans[8,20].

Notably, climatological mean state in South America has undergone changes due to natural long-term variability (e.g., AMO and IPO) both/or global warming[21–25]. For example, precipitation in the Amazon basin[24,25] has increased, leading to higher water levels and increased discharge in the Amazon River, reflecting heightened local hydrological activity[26]. Concurrently, the South America low-level jet (SALLJ[27]), which traverses the continent from north to south along the Andes Mountains, has experienced intensification[21,23]. This intensified SALLJ brings abundant moisture from the Amazon basin, resulting in increased precipitation across central to southeastern South America. These changes align with the southward shift of the South Atlantic Convergence Zone (SACZ), which follows the movement of the South Atlantic Subtropical High (SASH[22]).

The strengthened SALLJ in recent decades have led to an intensified atmospheric linkage between tropical and subtropical South America[20]. It implies that subtropical South America could have more opportunities to communicate with other regions such as tropical Pacific (e.g., ENSO) via its stronger connection with tropical South America. However, despite well-known ENSO teleconnections toward South America through tropics and extratropicas[28], the reversal linkages warrant further investigation and clarification.

In this context, we found that the interannual variability of SACZ and its related atmospheric circulation has a significant connection with the ENSO over recent decades. Building upon these findings, we aim to get insight into whether the recent emergence of significant SACZ–ENSO connection stems from the long-term natural variability[24,25,29,30] (such as AMO and IPO) or from global warming trends[31,32]. By analyzing the future global warming simulations from CMIP6, we found that the connection between SACZ and ENSO is projected to strengthen further in future global warming scenarios. This leads us to conclude that the observed strengthened link between SACZ and ENSO is plausibly linked to global warming rather than being exclusively ascribed to natural variability.

Emergence of SACZ and ENSO connection in observations

To discern the prevailing interannual variability pattern of precipitation across South America, the Empirical Orthogonal Function (EOF, a.k.a., principal component analysis) is applied to the 900-monthly precipitation anomalies over 1948–2022. To focus our examination on interannual timescales, a 13-year high-pass filter is first applied before conducting the EOF analysis. It is noteworthy that the outcomes of this study are not sensitive to the selected window (e.g., 11- or 15-year).

The leading EOF mode of precipitation displays a meridional dipole pattern spanning tropical and subtropical South America (Fig. 1a). The center of positive precipitation anomalies is located over central to southeastern South America with a cyclonic circulation within the range of 25–60°W and 25–50°S. This configuration of positive precipitation anomalies seems to be tilted northwest-southeast from the continental center toward the South Atlantic, resembling the SACZ where subtropical mean precipitation is large (Supplementary Fig. 1). That is, the 1st EOF mode reflects the variability of SACZ. Concurrently, the center of negative precipitation anomalies is situated northward along the equator, particularly encompassing the northern sector of the Amazon basin extending towards the northwestern equatorial Atlantic. Consequently, this mode appears to be associated with a local meridional overturning circulation, involving ascent over the SACZ and subsidence over tropical northern South America (TNSA).

Figure 1b represents the principal component (PC) time series of the 1st EOF (a black line) and its 30-year running standard deviation (purple line) since 1950. This result indicates a discernible intensification in the variability of precipitation dipole, particularly post-1980. To further understand the variability of precipitation dipole, we obtained the SACZ and TNSA (red and blue box regions in Fig. 1a) precipitation time series. Figure 1c displays the 30-year running correlation between SACZ and TNSA precipitation in late spring (May-June-July, MJJ) due to a prominent intensifying trend during this season. Importantly,

similar results are obtained with other precipitation datasets, such as the ECMWF Reanalysis version 5 and the observation-based dataset of the Global Precipitation Climatology Project (GPCP). The constant increase in the negative correlation signifies an enhanced linkage between tropical and subtropical regions. Henceforth, we will refer to the time series of SACZ precipitation during MJJ as the SACZ index for convenience.

As mentioned above, previous studies have indicated the change in the climatological mean state. Keeping paced with, our investigation reveals an intensification in variability of precipitation dipole between tropical and subtropical South America (Fig. 1b-c), resembling SACZ. Based on the findings, we aim to explore whether or not the SACZ is linked to ENSO which is featured by the strongest interannual variability (Supplementary Fig. 2).

Subsequently, employing a 30-year running window, we executed a lagged correlation analysis between the SACZ (MJJ[0]) and ENSO (Nino-3.4; D[0]JF[1]) indices. Acknowledging ENSO's capacity to modify South American precipitation through atmospheric teleconnections[28], we first eliminate the previous winter ENSO signals from the SACZ index through linear regression before conducting further analysis. Notably, the influence of the preceding ENSO on SACZ in the subsequent MJJ season is limited, as indicated by the correlation coefficient below 0.2 and insignificance at a 95% confidence level.

Figure 1d describes the result of 30-year running lead-lagged correlation coefficients between SACZ and following ENSO indices. Notably, there is an increasing trend. Consequently, the SACZ-leading-ENSO correlation becomes significant at a 95% confidence level since mid-1980s, with a maximum correlation coefficient of about 0.6 around 2000s. These results indicate that SACZ precedes ENSO with a 7-month lead. Note that similar results are obtained when other datasets such as ERA5 and GPCP are utilized, which underscores the robust emergence of the SACZ–ENSO connection in recent decades.

To understand how the SACZ leads the ENSO in recent decades, anomalies of SST, low-level wind, and precipitation from AMJ[0] to D[0]JF[1] are regressed on the SACZ index (MJJ[0]) during the last three decades (1992–2022) (Fig. 2a-e; see also Supplementary Fig. 3 for 1948–1978). Here, we note that when same analysis is applied into other reanalysis datasets, analogous patterns are obtained (Supplementary Figs. 4 and 5). In AMJ[0] and MJJ[0] (Fig. 2a-b), there are northeasterly wind anomalies over TNSA and northwesterly wind anomalies (i.e., SALLJ) over central South America. With the enhanced moisture transport by the anomalous northerly wind, precipitation increased over the SACZ and decreased over TNSA to the equatorial Atlantic. Simultaneously, northeasterly wind anomalies along the eastern coast of southern Brazil drive moisture supply from the ocean, inducing more precipitation along the SACZ.

When the precipitation dipole over South America is the most evident (MJJ[0]), a meridional overturning circulation clearly appears over South America (Fig. 2f), wherein low-level northerly wind over the southern hemisphere corresponds to the SALLJ. Simultaneously, the negative precipitation anomalies over the TNSA to equatorial Atlantic modify the Walker circulation by convection (Fig. 2g). This, in turn, results in amplified precipitation over the equatorial central Pacific with westerly wind anomalies. These

anomalies drive SSTA warming by propagating downwelling oceanic Kelvin waves across the equatorial Pacific. In JJA[0], the precipitation dipole and northerly wind anomalies over tropical South America exhibit reduced intensity. While the positive precipitation anomalies with westerly wind anomalies over the equatorial Pacific are intensified further through the Bjerknes feedback, developing an El Niño event until following winter (Fig. 2c-e).

Simulated SACZ-ENSO relationship in Historical runs of CMIP6

The results obtained from the observational reanalysis dataset indicate that the lagged connection between SACZ and ENSO tends to be constantly enhanced since late 20th century (Fig. 1d). To get insight into whether the lagged SACZ–ENSO connection arises from the long-term natural variability[24,25,29,30] (e.g., AMV and IPO) or from anthropogenic forcing[31,32], we further investigate the SACZ–ENSO relationship using historical and SSP585 simulations from the CMIP6 datasets.

We first examined the climatological mean states over South America in the Historical simulation from a multi-model ensemble (MME) perspective. It is found that large-scale climatological features such as Atlantic ITCZ, SACZ, SALLJ, and South Atlantic Subtropical High are well captured although its amplitude is somewhat small (Supplementary Fig. 6).

Next, the lagged relationship between SACZ and ENSO in the Historical simulations was investigated. Herein, the indices are defined by the same method applied into the observational analysis (refer to the Method). Grey bars in Fig. 3a shows the lagged correlation coefficients between SACZ (MJJ[0]) and ENSO (D[0]JF[1]) indices across each climate model. The range spans from the highest coefficient of 0.369 in CanESM5 to the lowest of -0.050 in TaiESM1. 30 among 35 climate models (83.3%) exhibit the positive correlation, thus confirming a significant positive relationship. Likewise, the MME is 0.108 (black bar), seemingly small but significant at a 99% confidence level by the Student *t*-test. This result indicates that SACZ can lead ENSO in the Historical simulations.

Additionally, Fig. 3b (left panel) depicts that the MME of lagged correlation coefficients between SACZ and ENSO with a 30-year running window. Here, the temporal mean is about 0.1, akin to the MME in Fig. 3a. Remarkably, there is a small interdecadal variability without a prominent trend over the period, implying limited external forcings.

Subsequently, we explored how SACZ leads ENSO in the Historical simulation. To this end, lagged regression analysis with the SACZ index is conducted. In AMJ[0] to JJA[0] (Supplementary Fig. 7), SACZ is well organized with SALLJ over the central South America with a cyclonic circulation over the La Plata basin. Simultaneously, anomalous negative precipitation with easterly winds prevails along the equator from tropical South America to Atlantic. Over the equatorial Pacific, there are westerly wind with positive precipitation anomalies, accompanying a weak SSTA warming. Although the SACZ weakens subsequently, the Bjerknes feedback mechanism over the equatorial Pacific continues to foster ENSO development in the ensuing season, rendering outcomes comparable to observations.

Enhanced SACZ–ENSO connection under global warming scenario (SSP585)

Next, the relationship between SACZ and ENSO in SSP585 is examined. Figure 3a provides their lagged correlation coefficients across 27 climate models (pink bars), with values ranging from the highest coefficient of 0.413 in CMCC-CM2-SR5 to the lowest of -0.059 in AWI-CM-1-1-MR. The MME is 0.206 (red bar), approximately twice of Historical simulations, significant at a 99% confidence level. 26 among 27 climate models (96.3%) shows a positive SACZ–ENSO relationship, indicating its significance.

Figure 3b (right panel) indicates the MME of 30-year running lagged correlation coefficients between the SACZ and ENSO indices over the 2015–2100, wherein it is found that their connection gets intensified as the anthropogenic forcing increases. This result indicates that anthropogenic forcing, rather that natural long-term variability, is responsible for the intensified SACZ–ENSO connection. It also implies that the observed emergence of SACZ–ENSO connection during recent decades can be largely interpreted as a result of global warming.

We tried to further investigate how SACZ leads ENSO by a lead-lagged regression analysis with the SACZ index (Supplementary Fig. 7). Similar to the Historical simulations, distinct positive and negative precipitation anomalies manifest over SACZ and the tropical South America to equatorial Atlantic in AMJ[0], of which pattern accompanies anti-cyclonic and cyclonic circulation over the northern and southern region of SACZ. Note that those patterns exhibit a pronounced southeastward extension in SSP585, compared to those of Historical simulations (Fig. 4a). As a result, increase and decrease in precipitation over SACZ and equatorial Atlantic in prominent. Simultaneously, the Walker circulation over the Pacific is effectively modulated, so that westerly wind anomalies couple with positive precipitation anomalies emerge over the equatorial Pacific. This configuration serves as a trigger for ENSO events, as persisting until summer season.

Likewise, the enhanced SACZ–ENSO connection is also verified when the first (2015–2045) and last 30-year (2070–2100) of SSP585 simulations are compared to each other (Supplementary Fig. 8). This result can also be inferred by the result of Fig. 3b.

The role of climatological mean state change in SACZ-ENSO connection

We further investigate how the climatological mean state and variability in the SSP585 differs from those of the Historical simulations, and try to understand the role of modified climatology in the SACZ-ENSO connection. Figure 4b indicates the difference of climatological mean precipitation and low-level wind in MJJ season between SSP585 and Historical simulations. Herein, it is known that northerly wind over South America gets intensified, and cyclonic circulation is clearly formed over the southeastern South America. As a result, precipitation increases over the continents to mid-latitude South Atlantic. This result represents that SACZ gets enhanced as displaced poleward and expanded eastward. Simultaneously,

there is prominent precipitation reduction along the equatorial Atlantic, implying weakened local Hadley circulation over the South America to South. According to the climatological mean state change, variability of precipitation is also increased along the axis of SACZ (Fig. 4c).

Note that the modified pattern of climatological mean state (Fig. 4b) is considerably similar to that of variability (Fig. 4c) and enhanced effect of SACZ on ENSO (Fig. 4a). These results imply that the strengthened variability of SACZ is tightly linked to the equatorial Atlantic under modified climatological mean state, which favors further connection to the tropical Pacific.

Discussion

So far, we examined the effect of the SACZ on the ENSO development and found that the SACZ–ENSO connection gets intensified over the last half century by analyzing the observational reanalysis dataset. During recent decades, SACZ variability accompanies anomalous meridional overturning circulation over the continent, forming convective precipitation anomalies over the tropical south America to Atlantic. The anomalous convective precipitation modulates the Walker circulation over the Pacific to Atlantic, triggering ENSO events.

It is acknowledged that ENSO affects mid-latitude South America through extratropical atmospheric teleconnection[28]. Our results imply that the mid-latitude South America also influences on ENSO, implying efficient two-way interactions under the global warming. Additionally, since the ENSO events are projected to be stronger and occur more frequently under global warming period [15], making it more influential to our lives[33]. Thus, we believe our findings contribute valuable insights into the intricate dynamics governing ENSO development in future.

Additionally, our finding has unveiled an intensified lagged SACZ–ENSO connection in the future global warming scenario by analyzing CMIP6 datasets. This enhancement is attributed to the amplified wetness of South America, driven by an intensified SALLJ. As a result, SACZ can be displaced southward, so that there will be a remarkable precipitation dipole between SACZ and tropical South America to Atlantic. That is, we identify anthropogenic forcing as a primary driver behind the reinforced SACZ-ENSO connection.

Nonetheless, we cannot exclude the role of natural variability in the recent SACZ–ENSO connection. Particularly, when the Southern Hemisphere becomes warmer than the Northern Hemisphere, the Atlantic ITCZ can be displaced equatorward. Simultaneously, the SACZ as well as South Atlantic Subtropical High move southward. This background change by natural long-term variability such as IPO and AMO provides a favorable condition for the enhanced connection between SACZ and ENSO.

It is worthwhile to note that Atlantic-Niño has the potential to trigger ENSO events, and it is reported that SALLJ can significantly lead Atlantic-Niño during recent decades. Given the observed relationship between SALLJ and SACZ, it is beneficial to examine the relationship between SACZ and Atlantic-Niño. The lagged correlation coefficients between SACZ in MJJ and Atlantic-Niño in JJA gets greater over 1948–2022, so that it reaches − 0.50 during last three decades. It implies that the SACZ with SALLJ

significantly modulates Atlantic-Nino in summer during recent decades, and the whole system over South America to Atlantic leads ENSO events in the following winter. Subsequently, we examined the correlation between Atlantic-Niño and ENSO in the climate models. However, we found that their correlation is not significantly changed in the future scenario (Supplementary Fig. 9). This result implies that SACZ rather than Atlantic-Niño will be more influential to ENSO in the future.

Method

Reanalysis Dataset. We utilized the monthly dataset of the U.S. NOAA National Center for Environmental Prediction Reanalysis 1 (NCEP-R1), which is an assimilated dataset that uses a state-of-the-art analysis and forecast system, spanning from 1948 to the present. For SSTs, NOAA's Extended Reconstruction Sea Surface Temperature version 5 (ERSSTv5) are selected, which is a global monthly SST dataset derived from NOAA's International Comprehensive Ocean-Atmosphere Dataset (ICOADS), available from 1854 to the present. For NCEP-R1 and ERSSTv5, the analysis period in this study was from 1948 to 2022. Also, ERA5[34] reanalysis dataset (1950–2021) is also selected to confirm the robustness of the results. In addition, Global Precipitation Climatology Project (GPCP) Monthly Analysis Product (1979–2022) are also analyzed since it provides a consistent analysis of global precipitation from an integration of various satellite data sets over land and ocean and a gauge analysis over land.

CMIP6 Dataset. For Historical simulations, we can retain 35 climate models which have SST, SLP, wind, and precipitation. For SSP585 simulations, we can reserve 27 climate models which have SST, SLP, wind, precipitation.

Table 1
List of CMIP6 climate models used in this study. In each climate models, SST, precipitation, low-level wind (U, V) dataset are reserved.

Historical	SSP585
ACCESS-CM2	ACCESS-CM2
ACCESS-ESM1-5	ACCESS-ESM1-5
AWI-CM-1-1-MR	AWI-CM-1-1-MR
BCC-CSM2-MR	BCC-CSM2-MR
BCC-ESM1	CanESM5
CAMS-CSM1-0	CESM2
CanESM5	CESM2-WACCM
CESM2	CMCC-CM2-SR5
CESM2-FV2	E3SM-1-1
CESM2-WACCM	EC-Earth3
CESM2-WACCM-FV2	EC-Earth3-Veg
CMCC-CM2-SR5	EC-Earth3-Veg-LR
E3SM-1-0	FGOALS-f3-L
E3SM-1-1	FGOALS-g3
E3SM-1-1-ECA	FIO-ESM-2-0
EC-Earth3-Veg	GFDL-ESM4
EC-Earth3-Veg-LR	INM-CM4-8
FGOALS-f3-L	INM-CM5-0
FGOALS-g3	IPSL-CM6A-LR
FIO-ESM-2-0	KACE-1-0-G
GFDL-ESM4	MIROC6
INM-CM4-8	MPI-ESM1-2-HR
INM-CM5-0	MPI-ESM1-2-LR
IPSL-CM6A-LR	MRI-ESM2-0
MCM-UA-1-0	NESM3

Historical	SSP585
MIROC6	NorESM2-LM
MPI-ESM1-2-HR	NorESM2-MM
MPI-ESM1-2-LR	
MRI-ESM2-0	
NESM3	
NorCPM1	
NorESM2-LM	
NorESM2-MM	
SAM0-UNICON	
TaiESM1	

Declarations

Data availability. All observational dataset and CMIP6 dataset can be downloaded from open URL. NCEP-R1:https://psl.noaa.gov/data/gridded/data.ncep.reanalysis.html.
ERSSTv5: https://www.esrl.noaa.gov/psd/data/data.php and
https://www.metoffice.gov.uk/hadobs/hadisst/data/download.html, and
ERA5: https://www.metoffice.gov.uk/hadobs/hadisst/data/download.html. GPCP: https://esgf-node.llnl.gov/projects/cmip6/. CMIP6: https://esgf-node.llnl.gov/projects/cmip6/.

Index. ENSO index is represented by SSTA averaged over the Niño-3.4 region (120°W–170°W and 5°S–5°N), wherein DJF season is focused on. The SACZ index is defined by the areal averaged precipitation anomalies over the SACZ region (45–65°W, 10–30°S) in MJJ season. For the SACZ index, a high-pass filter (13-year) is first applied to emphasize interannual variability, and the previous winter (DJF) ENSO signal was removed linearly using linear regression analysis against the ENSO index in order to exclude previous winter ENSO effects.

Code availability. Codes used in the manuscript are available upon reasonable requests from J.-H. Park (jhp11010@gmail.com).

Acknowledgments. J.-H. Park was supported by the National Research Foundation of Korea (NRF) grant funded by the Korea government (MSIT) (NRF-2023R1A2C1004083 and RS-2023-00219830). J.-S. Kug was supported by the National Research Foundation of Korea (NRF) grant funded by the Korean government (NRF-2022R1A3B1077622).

Author Contributions J.-H. Park conceived the idea and shared it with other coauthors. J.-H. Park conducted the analyses and prepare the figures with H.-J. Park. All coauthors thoroughly revised the manuscript which was first written by J.-H. Park. All coauthors participated in the discussion on the results.

Competing interests The authors declare no competing interests.

References

1. Schneider, T., Bischoff, T. & Haug, G. H. Migrations and dynamics of the intertropical convergence zone. *Nature* **513**, 45–53 (2014).
2. Carvalho, L. M. V., Jones, C. & Liebmann, B. The South Atlantic convergence zone: Intensity, form, persistence, and relationships with intraseasonal to interannual activity and extreme rainfall. *J. Clim.* **17**, 88–108 (2004).
3. Robertson, A. W. & Mechoso, C. R. Interannual and interdecadal variability of the South Atlantic convergence zone. *Mon. Weather Rev.* **128**, 2947–2957 (2000).
4. Soares-Filho, B. S. *et al.* Modelling conservation in the Amazon basin. *Nature* **440**, 520–523 (2006).
5. Dirzo, R. & Raven, P. H. Global state of biodiversity and loss. *Annu. Rev. Environ. Resour.* **28**, 137–167 (2003).
6. Wang, C. An overlooked feature of tropical climate: Inter-Pacific-Atlantic variability. *Geophys. Res. Lett.* **33**, 1–5 (2006).
7. Builes-Jaramillo, A., Marwan, N., Poveda, G. & Kurths, J. Nonlinear interactions between the Amazon River basin and the Tropical North Atlantic at interannual timescales. *Clim. Dyn.* **50**, 2951–2969 (2018).
8. Ham, Y.-G. *et al.* Inter-Basin Interaction Between Variability in the South Atlantic Ocean and the El Niño/Southern Oscillation. *Geophys. Res. Lett.* **48**, e2021GL093338 (2021).
9. Rodrigues, R. R., Haarsma, R. J., Campos, E. J. D. & Ambrizzi, T. The impacts of inter-El Niño variability on the tropical Atlantic and northeast Brazil climate. *J. Clim.* **24**, 3402–3422 (2011).
10. Yim, B. Y., Yeh, S.-W., Song, H.-J., Dommenget, D. & Sohn, B. J. Land-sea thermal contrast determines the trend of Walker circulation simulated in atmospheric general circulation models. *Geophys. Res. Lett.* **44**, 5854–5862 (2017).
11. Lewis, S. L., Brando, P. M., Phillips, O. L., Van Der Heijden, G. M. F. & Nepstad, D. The 2010 Amazon drought. *Science (80-.).* **331**, 554 (2011).
12. Fu, R., Dickinson, R. E., Chen, M. & Wang, H. How do tropical sea surface temperatures influence the seasonal distribution of precipitation in the equatorial Amazon? *J. Clim.* **14**, 4003–4026 (2001).
13. SWAP, R., GARSTANG, M., GRECO, S., TALBOT, R. & KÅLLBERG, P. Saharan dust in the Amazon Basin. *Tellus B* **44**, 133–149 (1992).
14. Timmermann, A. *et al.* El Niño–Southern Oscillation complexity. *Nature* **559**, 535–545 (2018).

15. Cai, W. *et al.* Changing El Niño–Southern Oscillation in a warming climate. *Nat. Rev. Earth Environ.* (2021). doi:10.1038/s43017-021-00199-z
16. Zebiak, S. E. Air–Sea Interaction in the Equatorial Atlantic Region. *J. Clim.* **6**, 1567–1586 (1993).
17. Keenlyside, N. S. & Latif, M. Understanding Equatorial Atlantic Interannual Variability. *J. Clim.* **20**, 131–142 (2007).
18. Power, S., Casey, T., Folland, C., Colman, A. & Mehta, V. Inter-decadal modulation of the impact of ENSO on Australia. *Clim. Dyn.* **15**, 319–324 (1999).
19. Kerr, R. A. A North Atlantic Climate Pacemaker for the Centuries. *Science (80-.).* **288**, 1984 LP – 1985 (2000).
20. Park, J.-H. *et al.* Distinct decadal modulation of Atlantic-Niño influence on ENSO. *npj Clim. Atmos. Sci.* **6**, 105 (2023).
21. Jones, C. Recent changes in the South America low-level jet. *npj Clim. Atmos. Sci.* **2**, 20 (2019).
22. Zilli, M. T., Carvalho, L. M. V. & Lintner, B. R. The poleward shift of South Atlantic Convergence Zone in recent decades. *Clim. Dyn.* **52**, 2545–2563 (2019).
23. Montini, T. L., Jones, C. & Carvalho, L. M. V. The South American Low-Level Jet: A New Climatology, Variability, and Changes. *J. Geophys. Res. Atmos.* **124**, 1200–1218 (2019).
24. Wang, X. Y., Li, X., Zhu, J. & Tanajura, C. A. S. The strengthening of Amazonian precipitation during the wet season driven by tropical sea surface temperature forcing. *Environ. Res. Lett.* **13**, (2018).
25. Friedman, A. R., Bollasina, M. A., Gastineau, G. & Khodri, M. Increased Amazon Basin wet-season precipitation and river discharge since the early 1990s driven by tropical Pacific variability. *Environ. Res. Lett.* **16**, (2021).
26. Gloor, M. *et al.* Intensification of the Amazon hydrological cycle over the last two decades. *Geophys. Res. Lett.* **40**, 1729–1733 (2013).
27. Marengo, J. A., Soares, W. R., Saulo, C. & Nicolini, M. Climatology of the low-level jet east of the Andes as derived from the NCEP-NCAR reanalyses: Characteristics and temporal variability. *J. Clim.* **17**, 2261–2280 (2004).
28. Cai, W. *et al.* Climate impacts of the El Niño–Southern Oscillation on South America. *Nat. Rev. Earth Environ.* **1**, 215–231 (2020).
29. Silva, C. B., Silva, M. E. S. & Ambrizzi, T. Climatic variability of river outflow in the Pantanal region and the influence of sea surface temperature. *Theor. Appl. Climatol.* **129**, 97–109 (2017).
30. Jones, C. & Carvalho, L. M. V. The influence of the Atlantic multidecadal oscillation on the eastern Andes low-level jet and precipitation in South America. *npj Clim. Atmos. Sci.* **1**, 1–7 (2018).
31. Russell, A. M., Gnanadesikan, A. & Zaitchik, B. Are the central andes mountains a warming hot spot? *J. Clim.* **30**, 3589–3608 (2017).
32. Carvalho, L. M. V. & Jones, C. CMIP5 simulations of low-level tropospheric temperature and moisture over the tropical americas. *J. Clim.* **26**, 6257–6286 (2013).

33. Yang, Y.-M., Park, J.-H., An, S.-I., Wang, B. & Luo, X. Mean sea surface temperature changes influence ENSO-related precipitation changes in the mid-latitudes. *Nat. Commun.* **12**, 1495 (2021).
34. Hersbach, H. *et al.* The ERA5 global reanalysis. *Q. J. R. Meteorol. Soc.* **146**, 1999–2049 (2020).

Figures

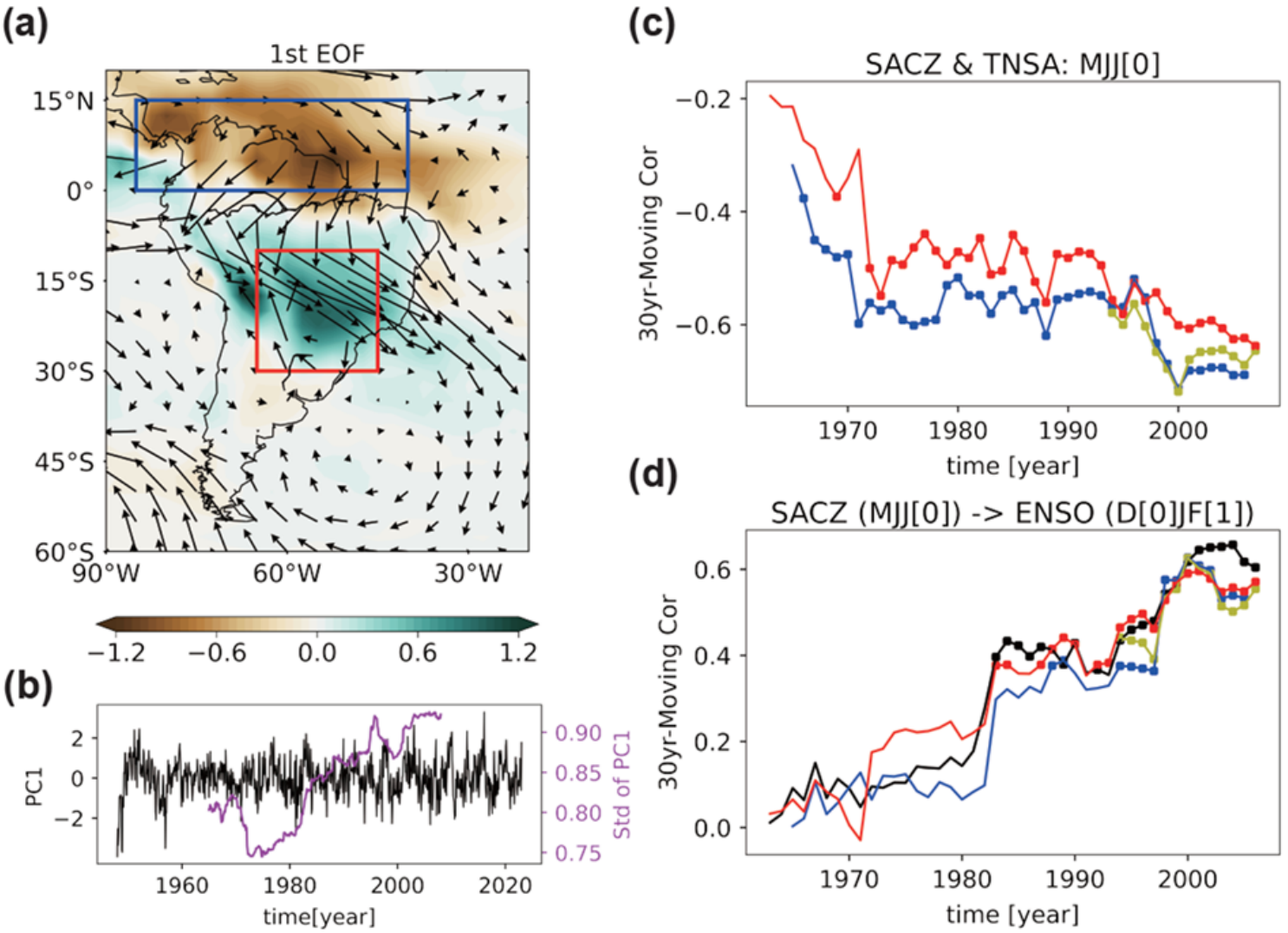

Figure 1

SACZ and its connection to ENSO. (a) The 1st EOF mode of 900-monthly precipitation anomalies (shading) over the South America from NCEP-R1 (1948-2022), which explains 6.6% of its total variability. Regressed low-level wind anomalies (at 850hPa) onto its PC time series are indicated by vectors. Herein, red and blue boxes indicate the regions of SACZ (45–65°W, 10–30°S) and tropical northern South America (TNSA) (40–85°W, 0–15°N), respectively. (b) The principal component (PC) time series of the 1st EOF mode (black line), and its 30-year running standard deviation since 1950 (purple line). (c) The 30-year running correlation between SACZ and TNSA precipitation index in MJJ[0]. The red, blue, and yellow lines indicate results obtained from NCEP-R1 (1948-2022), ERA5 (1950-2021), and GPCP datasets (1979-

2022). (d) The black line indicates 30-year running correlation coefficients between the 1st PC time series (black line in (b)) in MJJ[0] and ENSO index in D[0]JF[1]. The red, blue, and yellow lines indicate 30-year running correlation coefficient between SACZ (MAM[0]) and ENSO (D[0]JF[1]) index from NCEP-R1 (red), ERA5 (blue), and GPCP datasets (yellow). The rectangular marks in (c) and (d) represent significance at a 95% confidence level by Student's *t*-test (df = N-2).

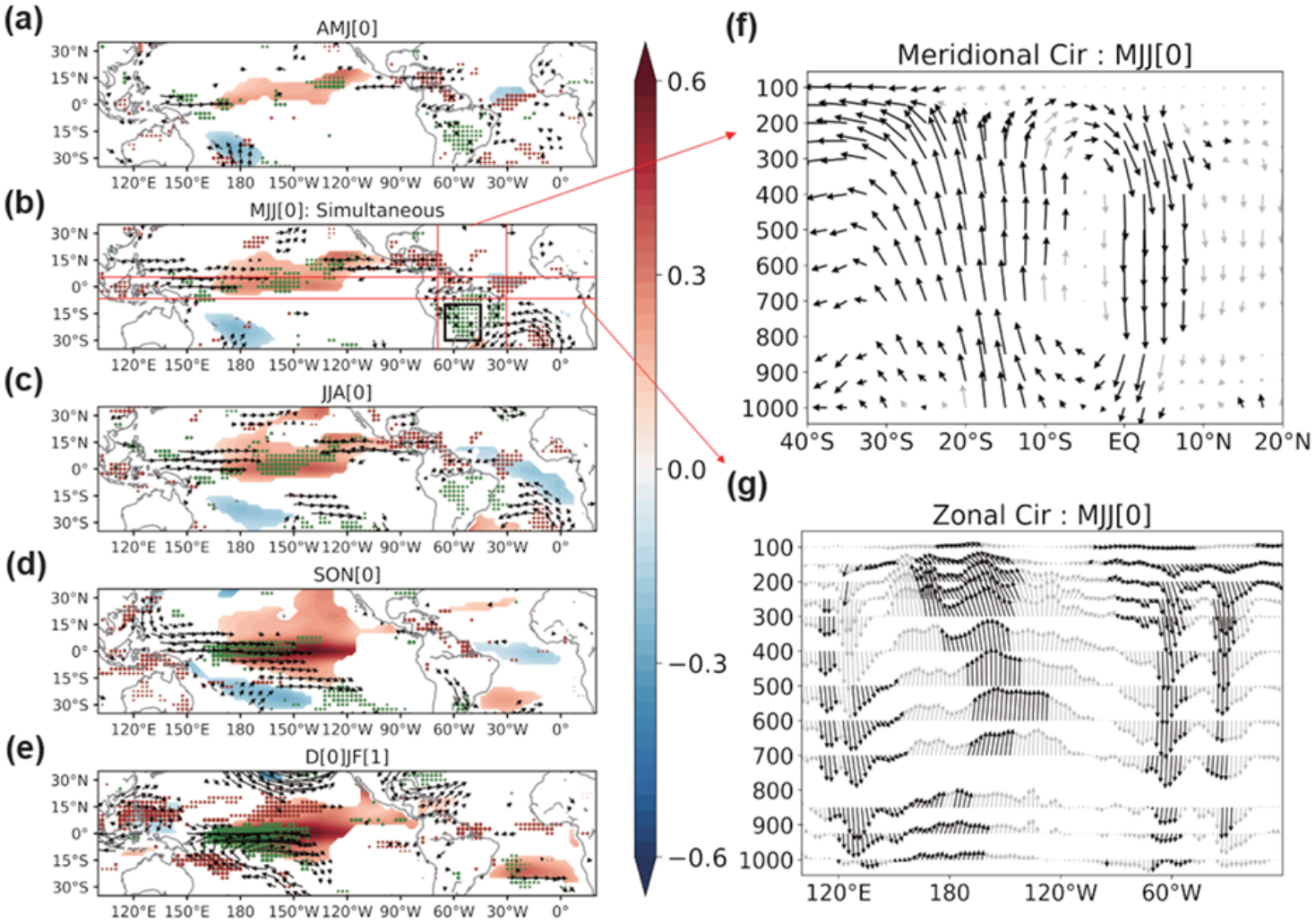

Figure 2

ENSO evolution associated with SACZ. (a) Regressed SSTAs (°C, shading bar at right), low-level wind anomalies (vector, at 850 hPa), and precipitation anomalies (dots, green and brown for positive and negative) in AMJ[0] against the SACZ index (MJJ[0]) during 1992-2022. (b)-(e) Same as (a), but in MJJ[0], JJA[0], SON[0], and D[0]JF[1], respectively. The SSTA, winds, and precipitation reflect a 95% confidence level by Student's *t*-test (df = N-2). (f) Regressed meridional overturning circulation in MJJ[0] by longitudinal averaged meridional wind (V) and vertical wind (-Omega) over 30-70°W onto SACZ index. (g) Regressed zonal overturning circulation in MJJ[0] by latitudinal averaged zonal wind (U) and vertical wind (-Omega) over 5°S-5°N onto SACZ index. In (f)-(g), black vectors reflect a 95% confidence level by Student's *t*-test (df = N-2).

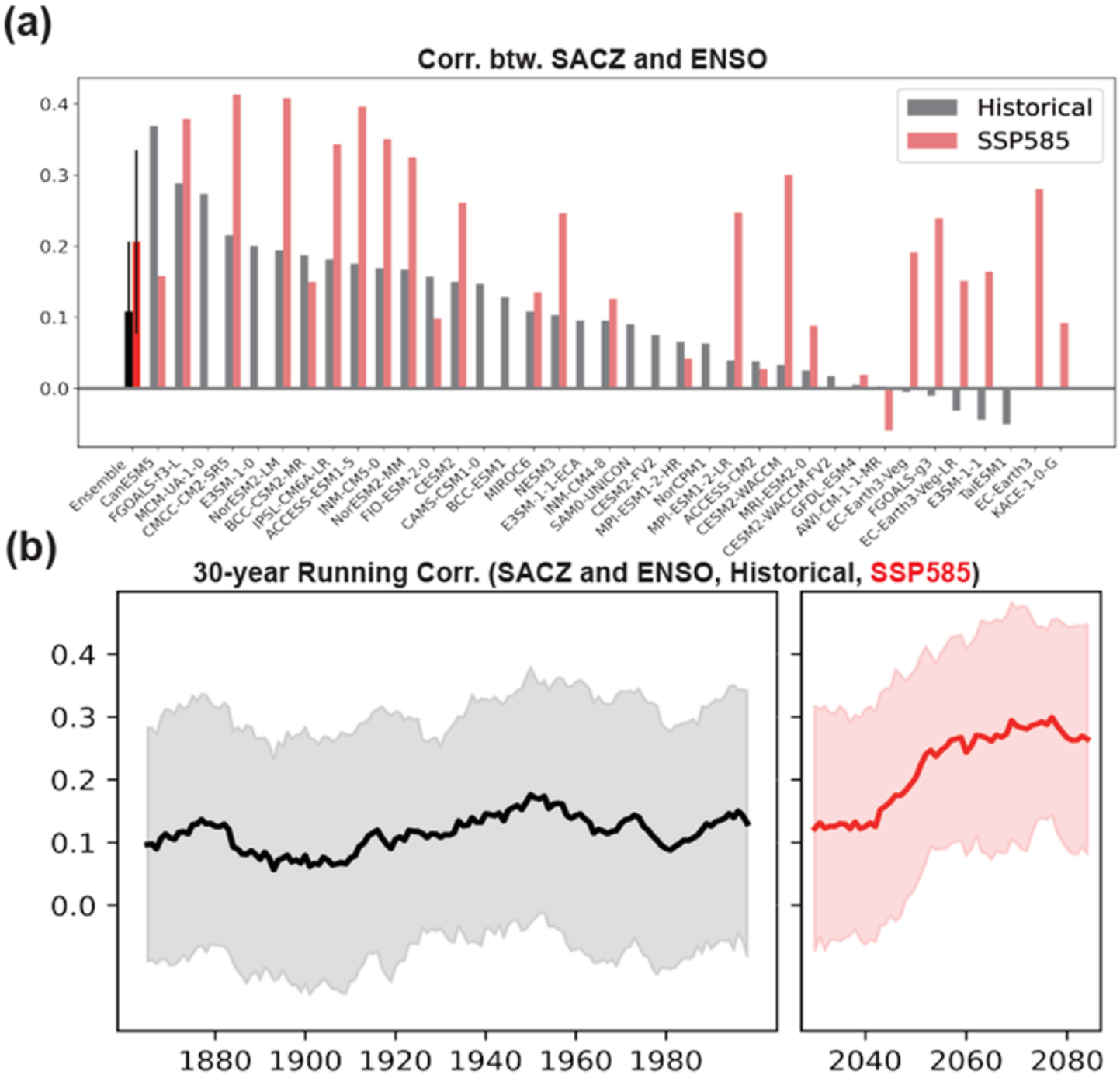

Figure 3

SACZ-ENSO Connection in Historical and SSP585 simulations from CMIP6. (a) Lagged correlation coefficients between SACZ index (MJJ[1]) and ENSO index (D[1]JF[2]) in the 35 and 27 climate models from Historical (grey, 1850-2014) and SSP585 (pink, 2015-2100) simulations in CMIP6. Their MMEs are illustrated at the leftmost in black and red color, wherein error bar indicates one standard deviation. (b) MME of 30-year running correlation coefficients between SACZ and ENSO index from Historical (black) and SSP585 (red) simulations in CMIP6. Grey and pink shadings indicate one standard deviation.

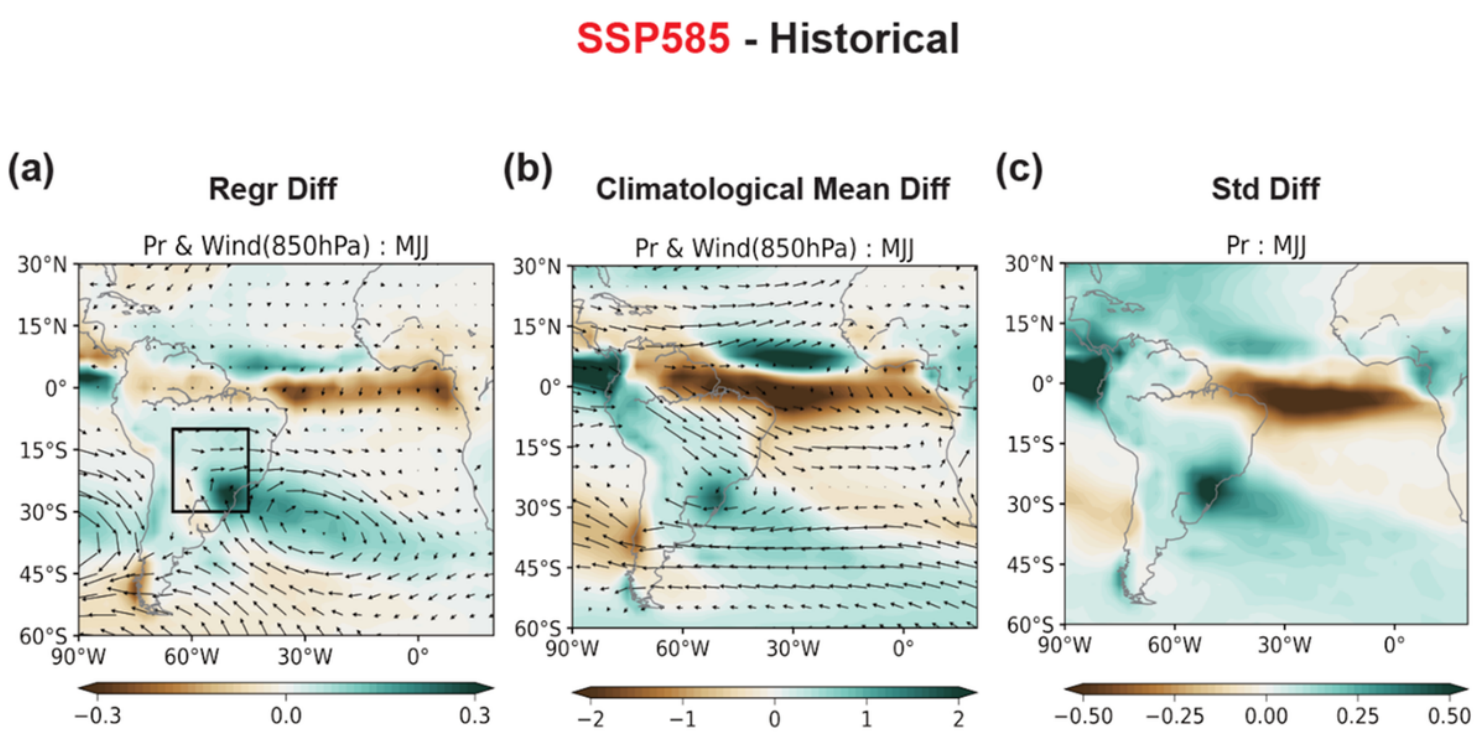

Figure 4

Differences of climatological mean state and standard deviation between SSP585 and Historical simulations and its effect on the modification of SACZ role. (a) Differences of regressed precipitation (shading) and low-level wind (850hPa, vectors) anomalies in MJJ season onto SACZ index between SSP585 and Historical simulations. (b) Differences of climatological mean precipitation (shading) and low-level wind (850hPa, vectors) in MJJ season between SSP585 and Historical simulations. (c) Differences of standard deviation of precipitation (shading) and low-level wind (850hPa, vectors) in MJJ season between SSP585 and Historical simulations.

Supplementary Files

This is a list of supplementary files associated with this preprint. Click to download.

- SACZENSOSupplementary20230922.docx